https://doi.org/10.2352/issn.2168-3204.2020.1.0.60

Image Quality Degradation Caused by Color Transformations in Multispectral Imaging—A Practical Review

Roy S. Berns, Munsell Color Science Laboratory, Program of Color Science, Rochester Institute of Technology, USA

Abstract

Conventional color imaging has three channels—R, G, and B. In multispectral imaging within the visible spectrum, the number of channels increases in order to improve color accuracy and estimate spectral reflectance factor. Image quality criteria important in multispectral imaging include colorimetric accuracy, sharpness, registration, and low noise. The color transformation matrix, connecting camera signals with CIE tristimulus values, affects color accuracy and the visibility of image noise and misregistration when the multiple channels are combined to a color-managed image. When the final goal is a color-accurate image for one set of illuminating and viewing conditions, the color transformation is often derived directly using nonlinear optimization minimizing the average color difference between spectrophotometer- and camera-based colorimetric coordinates. Optimization requires starting values and least squares minimizing spectral or tristimulus RMS error is typically used. Although it is effective for achieving convergence, the optimized matrix can result in a large reduction in image quality caused by noise propagation via the color transformation matrix. These concepts are reviewed.

Introduction

Imaging cultural heritage such as paintings, drawings, and sculptures has been in practice over 100 years. This includes silver halide photography, video, and current digital technologies. Common wavelength regions are UV, visible, infrared, and X-ray. This paper is limited to the visible spectrum using digital sensors.

Color cameras sample the visible spectrum in three regions, red, green, and blue or RGB. This is based on the trichromatic nature of color vision. Maxwell produced one of the earliest color imaging systems to prove the existence of trichromacy [1]. Ideally, the spectral sensitivities of RGB cameras are linear transformations of the eye's cone fundamentals, known as meeting the Luther-Ives (or Maxwell-Ives) condition [2, 3]. This results in perfect color accuracy for a single illuminant and a specific observer (e.g., the CIE 1931 standard observer). In practice, RGB sensors do not meet this condition because dyes cannot be manufactured with specific spectral absorptions and color accuracy is not the only quality criterion, described in detail below. An RGB system can be thought of as a three-channel system.

One method to improve color accuracy is to produce spectral images and calculate color-managed RGB from the spectra, equivalent to a spectrophotometer designed for color measurement. Estimating spectral reflectance factor requires increasing the number of channels. (Three sensors can only be used to estimate spectra accurately for materials colored with three or fewer colorants. See for example reference [4].) Increasing the number of channels can be accomplished by replacing RGB dyes of an area array sensor with four or more dyes. An RGB camera can be combined with multiple filters, lights, or both. For example, two different colored lights result in six channels. A panchromatic ("monochrome") sensor can be used with a multiplicity of colored filters, colored lights, or both. Finally, a panchromatic sensor can be used with a dispersing element such as a diffraction grating. When the number of channels is fewer than the number of reported wavelengths in a spectrophotometer, the term "multispectral" is used. When the number is much greater, the term "hyperspectral" is used. The ICC color management file format iccMAX [5] was designed for spectral data.

A second method to improve color accuracy is to increase the number of channels and derive a transformation where colorimetric coordinates are estimated directly from multispectral camera signals. This fits into the current ICC V2 and V4 file formats.

These two methods can lead to different transformations depending on the spectral sensitivities of the camera and the method of estimating the transformation. One consequence of this difference is a difference in spatial image quality. The purpose of this paper is to review the degradation in image quality caused by the multispectral color transformation.

Color Processing Pipeline

The processing pipeline in multispectral imaging, abbreviated "MSI", is transforming from raw camera signals to estimated spectral reflectance factor, $\hat{R}_\lambda$,shown in Eq.1 for j wavelengths, i colors, and n camera channels:

$$\hat{\mathbf{R}} = \mathbf{M}_S \mathbf{c}, \tag{1}$$

where

$$\hat{\mathbf{R}} = \begin{pmatrix} \hat{R}_{1,1} & \cdots & \hat{R}_{1,i} \\ \vdots & \cdots & \vdots \\ \hat{R}_{j,1} & \cdots & \hat{R}_{j,i} \end{pmatrix}, \mathbf{M}_S = \begin{pmatrix} a_{1,1} & \cdots & a_{1,n} \\ \vdots & \cdots & \vdots \\ a_{j,1} & \cdots & a_{j,n} \end{pmatrix},$$

$$\mathbf{c} = \begin{pmatrix} C_{1,1} & \cdots & C_{1,i} \\ \vdots & \cdots & \vdots \\ C_{n,1} & \cdots & C_{n,i} \end{pmatrix},$$

a are matrix coefficients, and C define radiometrically-linear camera signals that have been, successively, dark-current subtracted, corrected for spatial inhomogeneities in the sensor, lens, and lighting, and normalized to a reference white. (The normalization depends on the desired amount of "headroom" for specular highlights, typically around 95% of the maximum signal.)

A number of approaches have been used to determine the spectral transformation matrix [6] including a Moore-Penrose pseudoinverse, Wiener filtering, principal component analysis, and singular value decomposition, all using color targets as training data.

These are linear operations because the large number of matrix coefficients—the number of camera channels multiplied by the number of reference wavelengths—make convergence difficult using nonlinear optimization. The matrix shown in Eq. 1 results from a pseudoinverse, Eq. 2:

$$\mathbf{M}_S = \mathbf{c}^{+}\mathbf{R}, \tag{2}$$

where **R** is a matrix of reference spectral reflectance factor measurements and the superscript + indicates the pseudoinverse. Estimated tristimulus values are calculated from the spectral data, shown in Eq. 3:

$$\hat{\mathbf{t}} = \mathbf{T}_{xyz}\mathbf{S}\hat{\mathbf{R}}, \tag{3}$$

where

$$\mathbf{S} = \begin{pmatrix} S_1 & 0 & 0 \\ 0 & \ddots & 0 \\ 0 & 0 & S_j \end{pmatrix}, \mathbf{T}_{xyz} = \begin{pmatrix} \bar{x}_1 & \dots & \bar{x}_j \\ \bar{y}_1 & \dots & \bar{y}_j \\ \bar{z}_1 & \dots & \bar{z}_j \end{pmatrix},$$

$$\hat{\mathbf{t}} = \begin{pmatrix} \hat{X}_1 & \cdots & \hat{X}_i \\ \hat{Y}_1 & \cdots & \hat{Y}_i \\ \hat{Z}_1 & \cdots & \hat{Z}_i \end{pmatrix},$$

S_λ defines the spectral power distribution of the reference illuminant, and $\bar{x}_j\bar{y}_j\bar{z}_j$ define the color matching functions of the reference observer.

Tristimulus values are usually transformed to various color-managed RGB encodings. When processing images, the transformation from camera signals to color-managed linear RGB is a single concatenated matrix, shown in Eq. 4:

$$\hat{\mathbf{t}}_{RGB} = \mathbf{M}_{concatenated}\mathbf{c}, \tag{4}$$

where

$$\mathbf{M}_{concatenated} = \mathbf{M}_{RGB}^{-1}\mathbf{T}_{xyz}\mathbf{S}\mathbf{M}_S,$$

$$\mathbf{M}_{RGB} = \begin{pmatrix} X_r & X_g & X_b \\ Y_r & Y_g & Y_b \\ Z_r & Z_g & Z_b \end{pmatrix}, \hat{\mathbf{t}}_{RGB} = \begin{pmatrix} \hat{R}_1 & \cdots & \hat{R}_i \\ \hat{G}_1 & \cdots & \hat{G}_i \\ \hat{B}_1 & \cdots & \hat{B}_i \end{pmatrix}.$$

For clarity, normalization by the luminance factor (Y) of the perfect reflecting diffuser is not shown when calculating tristimulus values. This is accomplished by dividing $\mathbf{T}_{xyz}\mathbf{S}$ by the sum of row two of $\mathbf{T}_{xyz}\mathbf{S}$. The last steps are gamma correction and attaching an ICC profile.

The direct transformation from camera signals to tristimulus values is shown in Eq. 5:

$$\hat{\mathbf{t}}_{XYZ} = \mathbf{M}_T\mathbf{c}, \tag{5}$$

where

$$\mathbf{M}_T = \begin{pmatrix} a_{X,1} & \cdots & a_{X,n} \\ a_{Y,1} & \cdots & a_{Y,n} \\ a_{Z,1} & \cdots & a_{Z,n} \end{pmatrix}.$$

Nonlinear optimization is often used to estimate the transformation coefficients *a* comprising $\mathbf{M}_T$ where the average total color difference between spectrophotometer- and camera-based CIELAB values are minimized. For cameras that do not meet the Luther-Ives condition, minimizing total color difference improves color accuracy compared with estimating spectral reflectance factor (e.g., Eqs. 2 and 3).

Multispectral Image Quality

There are many ways to quantify image quality using both visual and computational techniques [7, 8]. Computational techniques measure image properties that, in turn, are transformed to metrics correlating with visual assessment. Quality criteria important in MSI include color accuracy, sharpness, registration, and low noise. Sharpness, registration and noise can be evaluated for each channel. Metrics that predict visual assessment are based on a color-managed image.

Color accuracy is quantified using calibration and verification targets, ideally having spectral properties similar to the artwork. There is an underlying assumption that high color accuracy for a calibration target leads to high color accuracy for the artwork. Metrics include the average, 90th percentile, and maximum of the total color differences of the color patches. Neutral samples should be analyzed separately to indicate neutral tracking and white balance. An example analysis is described in reference [9].

The recommended total color difference formula is CIEDE2000 [10] with the positional function, S_L, equal to unity [11]. CIEDE2000 is known as a weighted color-difference formula [12], shown in Eq. 5:

$$\Delta E_{00} = \sqrt{\left(\frac{\Delta L'}{k_L S_L}\right)^2 + \left(\frac{\Delta C'}{k_C S_C}\right)^2 + \left(\frac{\Delta H'}{k_H S_H}\right)^2 + R_T\left(\frac{\Delta C'}{k_C S_C}\right)\left(\frac{\Delta H'}{k_H S_H}\right)} \tag{5}$$

Positional functions, *S*, improve CIELAB's predictions of perceived color differences in the range of 0.5–5.0 ΔE^*_{ab}. Reciprocal weighting factors, *k*, are used when a specific application requires a different relative weighting of lightness, chroma, and hue differences. For imaging, it may be beneficial to have $k_C = 2$ since lightness and hue accuracy are often more critical than chroma accuracy.

Multispectral cameras have spectral sensitivities with narrower bandwidth across a greater wavelength range than an RGB camera. Lenses used for MSI must have minimal chromatic aberration (apochromatic) so that focusing is only required at a single channel. "Apochromatic" lenses designed for RGB imaging do not achieve this requirement [13]. A single focus results in both blurriness and image shifting. Blurriness is reduced by refocusing for each channel. The differences in focal length when refocusing lead to different magnification. Image shifting and magnification differences for the multiple channels are minimized by image registration. The channel

with spectral sensitivity most similar to the luminous efficiency function of the reference observer is used as the reference image.

Image sharpness and registration are quantified using slanted-edge targets in both the horizontal and vertical directions and in different locations across the image [14–16]. The spatial frequency response, *SFR*, of the slanted edge can be used to evaluate the focus of each channel. Perceived sharpness is evaluated using a color image. The image should be color managed (i.e., have an attached ICC profile) in order to calculate the *SFR* of a luminance channel, used to calculate acutance [8] that is correlated with perceived sharpness. Misregistration is defined as a shift in a line fit to the slanted edge compared with a reference channel. There is not a commonly used perceptual metric of misregistration.

Image noise results in a speckled or grainy appearance, in essence, unwanted variability in image regions known to be spatially uniform. In general, it is caused by properties of the sensor, electronics, and image processing. The standard deviation of neutral patches can be used as a measure of variability for each channel [16, 17]. Noise visibility in the color-managed image depends on the display, viewing distance, magnification, and image content. An alternative approach to quantify noise is to use all the patches of a color target. The total color difference between each pixel in a patch and the patch average is first calculated. These color differences are averaged, known as a mean-color-difference-to-the-mean, MCDM [12]. When using CIEDE2000, it is recommended that $S_L = 1$ and $k_C = k_H = 2$. This reduces the importance of chroma and hue noise compared with lightness noise, which is more visible. The statistics of these MCDMs are a measure of image noise. The critical values would be determined by viewing the image on a display under standardized magnification, viewing distance, display primaries and peak luminance.

The color transformation, ($\mathbf{T}_{xyz}\mathbf{SM}_S$) or $\mathbf{M}_T$, is another source of noise. Burns and Berns used multivariate error-propagation analysis to define noise in CIELAB units attributable to spectrophotometric and colorimetric measurement uncertainty [18]. These transformations were used to predict image noise resulting from seven-channel MSI [19]. Kuniba and Berns used the Burns and Berns research to define a noise parameter, *N*, that was used to evaluate photon shot noise in image sensors [20] and the tradeoffs between color accuracy and image noise when designing color filters for digital camera sensors [21, 22]. The noise parameter is given in Eq. 6:

$$N = \sqrt{\left(\Delta L^*_N\right)^2 + \left(\Delta a^*_N\right)^2 + \left(\Delta b^*_N\right)^2}, \tag{6}$$

where

$$\left(\Delta L^*_N\right)^2 \simeq \left(\frac{116A}{3}\right)^2 \left(a^2_{2,1} + a^2_{2,2} + \cdots + a^2_{2,n}\right),$$

$$\left(\Delta a^*_N\right)^2 \simeq \left(\frac{500A}{3}\right)^2 \left[\left(a_{1,1} - a_{2,1}\right)^2 + \left(a_{1,2} - a_{2,2}\right)^2 + \cdots + \left(a_{1,n} - a_{2,n}\right)^2\right],$$

$$\left(\Delta b^*_N\right)^2 \simeq \left(\frac{200A}{3}\right)^2 \left[\left(a_{2,1} - a_{3,1}\right)^2 + \left(a_{2,2} - a_{3,2}\right)^2 + \cdots + \left(a_{2,n} - a_{3,n}\right)^2\right],$$

$$A = \frac{Y^{-2/3}}{Y_n^{1/3}},$$

$$Y = 18.4 \quad (L^* = 50),$$

$$Y_n = 100,$$

and where the matrix row-sums are rescaled to unity before the calculation. Equation 6 is calculated for a medium gray sample under illuminant E (equal-energy spectrum). At $L^* = 50$, CIELAB and CIEDE2000 total color differences are identical. This is the gray-world assumption where all scene elements for all captured images integrate to a medium gray. Color transformation noise can also be calculated for each patch of a color target and the statistics analyzed. Achromatic noise is more visible than chromatic noise and a weighted color difference formula can be used, shown in Eq. 7 where the reciprocal weight, *k,* is greater than unity:

$$N_{(1:k:k)} = \sqrt{\left(\Delta L^*_N\right)^2 + \left(\frac{\Delta a^*_N}{k}\right)^2 + \left(\frac{\Delta b^*_N}{k}\right)^2} \tag{7}$$

Simulation

For the aims of this paper, camera signals and image rendering were calculated rather than experiment based.

Imai, Berns and collaborators [23–27] developed a two-filter MSI system using a Sinar 54 camera (22MP Kodak KAF-sensor 22000CE with its blue-green filter replaced with clear optical glass, Sinar P3 body, Sinaron apochromatic lens, and Sinar custom two-filter slider). Following extensive computations and one prototype, the final filters were BG39 (cyan) and GG475 (yellow), each glued with a visible bandpass filter. The camera could be used for both RGB imaging (with the cyan filter) and MSI. The normalized spectral sensitivities are plotted in Figure 1. These spectral sensitivities were used to calculate camera signals using the spectral irradiance of a Broncolor Pulso F4 with UVE protection dome Xenon strobe [28].

Three targets were used. The Xrite ColorChecker® Digital SG was used to derive transformation matrices. The Avian Rochester Next Generation Target [29] was used to evaluate color accuracy. Each patch's spectral reflectance factor was based on spectrophotometric measurements using 45°a/0° geometry. Colorimetric data were calculated for the CIE 1931 standard observer and illuminant D65.The third target was the MetaCow spectral image [30]. This is a 4200 x 6000 pixels computer-graphics rendered spectral image where the back half of a cow has the spectral reflectance factor of a patch from a Xrite ColorChecker® Classic while the front half is a theoretical metamer for illuminant D65 and the 1931 standard observer. The metamers' spectra were derived using published metameric blacks [31]. These metameric spectra result in extreme metamerism and as a consequence, the MetaCow is an excellent visualization target. In fact, metameric pairs are an alternate verification target, having high sensitivity to small differences in spectral sensitivity [32].

Equation 8 was used to calculate camera signals for each patch of the two targets and as image data for the MetaCow:

$$\mathbf{c} = \mathbf{T}_{msi}\mathbf{SR}, \tag{8}$$

where

$$\mathbf{T}_{msi} = \begin{pmatrix} \psi_{1,1} & \cdots & \psi_{j,1} \\ \vdots & \cdots & \vdots \\ \psi_{1,n} & \cdots & \psi_{j,n} \end{pmatrix},$$

and where ψ_j defines the spectral sensitivity of a multi-spectral channel, as shown in Figure 1. The spectral sensitivities were rescaled such that a perfect reflecting diffuser had camera signals of unity.

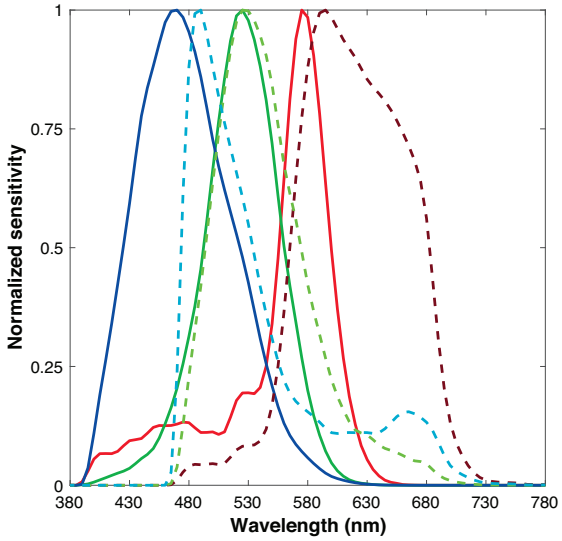

Figure 1. *Peak-height normalized spectral sensitivities of the multi-spectral camera used in this paper. Solid lines correspond to the cyan filter and dashed lines correspond to the yellow filter.*

The Matlab function *pinv*, a Moore-Penrose pseudoinverse, was used to derive $\mathbf{M}_S$ (Eq. 2). Because the transformation from spectral reflectance factor to tristimulus values is linear, using a pseudoinverse to derive $\mathbf{M}_T$ would result in the same transformation.

A better solution for $\mathbf{M}_T$ can be found using, for example, the Matlab nonlinear optimization function *fminunc,* to minimize the average $\Delta E_{00}(S_L = 1)$ using the ColorChecker Digital SG as the calibration target. This function is a variant of the Newton-Raphson method and as a result, convergence can occur at a local minimum rather than the true minimum. Accordingly, starting values are critical. Two sets of starting values were used. The first was the result from the pseudoinverse. The second set was a diagonal matrix for the cyan image with coefficients of 1, 1, and 2, and null values for the remaining coefficients. This matrix compensates for the high correlation between cyan and yellow filtered camera data, a result of the specific spectral sensitivities shown in figure 1. The coefficient of 2 led to a result closer to the true minimum than 1. (A value of 1 converged to a local minimum.)

The yellow-filtered RGB MetaCow image was manipulated in two ways. First, the image was shifted by one pixel in each direction. Second, a very small amount of Gaussian noise was added to the image. Thus, there were three different yellow-filtered images. Each optimal matrix was concatenated with the sRGB tristimulus matrix and used to calculate linear RGB images. These, in turn, were nonlinearly encoded and output as 16-bit sRGB encoded TIFF images.

Results and Discussion

The initial and optimized matrix coefficients, total-color-difference statistics for the Next Generation Target verification target, and the transformation noise for the initial and optimized matrices are shown in Tables I and II. The pseudo-inverse initial and optimized matrix coefficients did not change (at one significant figure). The average total color difference was 0.4, likely the minimum value. The six channels are nearly a linear transformation of color matching functions with a μ-factor of 0.96 [33]. (Perfect transformability has a μ = 1.) As such, minimizing tristimulus values RMS error led to a minimum average total color difference because RMS error was small. However, the pseudo-inverse resulted in a very large color-transformation noise of 27.4 (equivalent to $27.4\Delta E^*_{ab}$)! The a^* noise was particularly large. CIELAB a^* is calculated from rows one and two of the transformation matrix. The two green signals, one from each filter, result in very similar—but not identical— signals for the calibration target patches due to their very similar spectral sensitivities. The coefficients –4.6 and 4.7 in row one, having opposite sign, led to a small net contribution estimating tristimulus X, but a large contribution to transformation noise. Changing these two coefficients to 0.0 and 0.1 reduces the color-transformation noise to 11.5. This oscillation of the green channels also occurred in row three, but the coefficients were much smaller: –0.6 and 0.7; -0.2 and 0.2.

Table I. Nonlinear optimization initial and final matrices.

Pseudoinverse initial and final matrix	$\begin{pmatrix} 0.0 & -4.6 & 0.9 & -0.1 & 4.7 & 0.0 \\ 0.2 & -0.8 & 0.1 & 0.0 & 1.7 & -0.2 \\ -0.2 & -0.6 & 2.1 & 0.2 & 0.7 & -1.1 \end{pmatrix}$
Specific coefficients initial matrix	$\begin{pmatrix} 1 & 0 & 0 & 0 & 0 & 0 \\ 0 & 1 & 0 & 0 & 0 & 0 \\ 0 & 0 & 2 & 0 & 0 & 0 \end{pmatrix}$
Specific coefficients final matrix	$\begin{pmatrix} 0.6 & -0.1 & 0.2 & 0.4 & -0.1 & 0.0 \\ 0.5 & 0.7 & -0.2 & 0.2 & -0.2 & 0.0 \\ 0.0 & -0.2 & 1.8 & 0.1 & -0.1 & -0.5 \end{pmatrix}$

The diagonal coefficients matrix resulted in a very large average total color difference of 22.8 and color-transformation noise of 7.9. Following optimization, the average total color difference reduced to 0.5 and color-transformation noise reduced to 6.7. None of the matrix coefficients had large values and there was not sign oscillation for the green channels. The total color differences of each approach were not statistically significantly different at a 95% confidence interval based on the Student-T test.

The final matrices listed in Table I (with floating point precision) were used to render the MetaCow images, shown in Figure 2. Neither matrix resulted in perfect color accuracy. An additional source of error was the spectral differences between a Xenon strobe and illuminant D65. The magnitude and direction of difference were cow dependent.

The row four, column four MetaCow is shown in Figure 3. This cow is representative of all the other cows. The pseudoinverse-starting-values transformation resulted in a rendering where the pixel shift was quite evident. There is a red outline and the specular highlights vary from cyan to white to red. The addition of noise was also evident where there is appreciable red speckle. The specific-starting-values transformation did not have visible image shifting and the speckle was minor.

Table II. Color matrix transformation optimization results. Color difference data are for the independent verification target, the Next Generation Target.

Metric	Pseudo-inverse	Specific Coefficients
Before Optimization		
Average $\Delta E_{00}(S_L = 1)$	0.4	22.8
ΔL_N^* noise	2.2	1.2
Δa_N^* noise	26.9	7.3
Δb_N^* noise	4.7	2.9
N	27.4	7.9
Following optimization		
Average $\Delta E_{00}(S_L = 1)$	0.4	0.5
90th percentile $\Delta E_{00}(S_L = 1)$	0.7	1.0
Maximum $\Delta E_{00}(S_L = 1)$	2.0	2.4
ΔL_N^* noise	2.2	1.1
Δa_N^* noise	26.9	4.9
Δb_N^* noise	4.7	4.4
N	27.4	6.7

Figure 2. *(Top) Rendered MetaCow using the final pseudoinverse-based matrix. (Bottom) Rendered MetaCow using the final specific-coefficient-based matrix.*

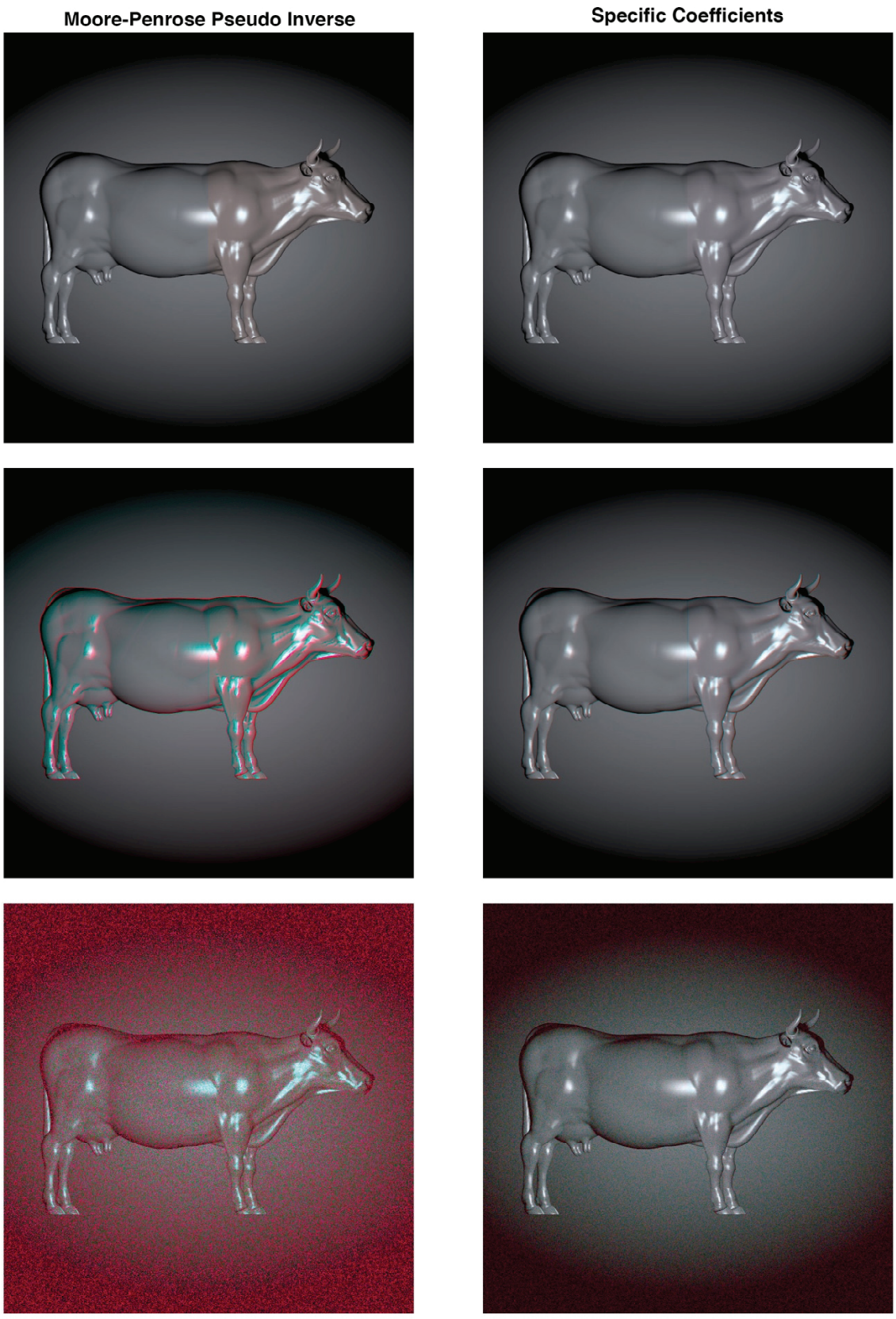

Figure 3. *Row four and column four MetaCow with the yellow image either unchanged (top), shifted by a single pixel in both directions (middle), or Gaussian noise added (bottom). The left column used the final matrix from the pseudoinverse starting values. The right column used the final matrix from the specific coefficients starting values.*

Conclusions

The current purpose of using MSI for documentation of cultural heritage is to improve color accuracy. It is well understood that adding channels improves color accuracy. However, this may come at a cost of reduced spatial image quality. The causes can be optical and computational. This paper has reviewed the image quality degradation caused by the color transformation linking camera signals with spectral reflectance factor or tristimulus values. This was demonstrated using simulations of a six-channel MSI system using an RGB sensor and cyan and yellow filters where the visibility of spatial degradation in the yellow-filtered image depended on the noise properties of the color transformation matrix. For this particular imaging system, a Moore-Penrose pseudoinverse was a poor choice for starting values when estimating a color transformation using optimization. Spatial image quality was improved by using a specific set of starting values. These were selected by analyzing the channel spectral sensitivities and recognizing that the green channel was largely unaffected by the choice of filters.

Colored LED illumination and a panchromatic sensor are sometimes used to build MSI systems. There are about 40 colored LEDs within the visible spectrum. When selecting specific LEDs, color transformation noise is equally important to color and spectral accuracy.

References

[1] J. Cat, Maxwell, Sutton, and the Birth of Color Photography: A Binocular Study. New York: Palgrave Pivot, 2013.

[2] H. E. Ives, "The transformation of color-mixture equations from one system to another," Journal Franklin Institute, vol. 16, pp. 673–701, 1915.

[3] A. C. Hardy and F. L. Wurzburg, "The theory of three-color reproduction," Journal of the Optical Society of America, vol. 38, pp. 227–240, 1937.

[4] R. S. Berns and M. J. Shyu, "Colorimetric characterization of a desktop drum scanner using a spectral model," Journal Electronic Imaging, vol. 4, pp. 360–372, 1995.

[5] ICC, ICC.2:2018 Image Technology Colour Management—Extensions to Architecture, Profile Format, and Data Structure, 2018.

[6] A. Ribés and F. Schmitt, "Linear inverse problems in imaging: An introductory survey," IEEE Signal Processing Magazine, vol. July, pp. 84–99, 2008.

[7] B. W. Keelan, Handbook of Image Quality: Characterization and Prediction. New York: Marcel Dekker, Inc., 2002.

[8] J. B. Phillips and H. Eliasson, Camera Image Quality Benchmarking. Chichester: John Wiley & Sons Ltd, 2018.

[9] R. S. Berns and S. Smith, "Analysis of color management default camera profiles for museum imaging applications," in Archiving 2012, Copenhagen: Society for Imaging Science and Technology, 2012, pp. 111–115.

[10] CIE, 15:2018 Colorimetry, 4th ed. Vienna: Commission Internationale de L'Éclairage, 2018.

[11] R. S. Berns, "Modification of CIEDE2000 for assessing color quality of image archives," in Archiving 2016, Washington: Society for Imaging Science and Technology 2016, pp. 181–185.

[12] R. S. Berns, Billmeyer and Saltzman's Principles of Color Technology, 4 ed. New Jersey: John Wiley & Sons, Inc., 2019.

[13] R. S. Berns, "Practical UV-VIS-NIR multispectral imaging," in *Archiving 2018*, Washington: Society for Imaging Science and Technology, 2018, pp. 47–52.

[14] P. D. Burns, "Using Slanted Edge Analysis for Color Registration Measurement," in Conference on Image Processing, Image Quality and Image Capture Systems (PICS-99), Savannah, Georgia, USA, April 25-28 1999, Savannah, 1999, pp. 51–53.

[15] ISO, ISO 12233:2017 Photography — Electronic still picture imaging — Resolution and spatial frequency responses. Geneva: International Organization for Standardization, 2017.

[16] ISO, ISO/TS 19264-1:2017 Photography -- Archiving systems -- Image quality analysis -- Part 1: Reflective originals. Geneva: International Organization for Standardization, 2017.

[17] ISO, ISO 15739:2017 Photography — Electronic still-picture imaging — Noise measurements. Geneva: International Organization for Standardization, 2017.

[18] P. D. Burns and R. S. Berns, "Error propagation in color signal transformations," Color Research and Application, vol. 22, pp. 280–289, 1997.

[19] P. D. Burns and R. S. Berns, "Image noise and colorimetric precision in multispectral image capture," in IS&T/SID Sixth Color Imaging Conference Scottsdale, 1998, pp. 83–85.

[20] H. Kuniba and R. S. Berns, "Spectral sensitivity optimization of color image sensors considering photon shot noise," Journal of Electronic Imaging, vol. 18, pp. 023002-1–023002-14, 2009.

[21] H. Kuniba and R. S. Berns, "The trade-off between color reproduction accuracy and image sensor noise," in IS&T/SID Sixteenth Color Imaging Conference, Portland, 2008, pp. 232–237.

[22] H. Kuniba and R. S. Berns, "Spectral sensitivity optimization of color image sensor considering photon shot noise," in SPIE Electronic Imaging Conference 6817, San Jose, 2008, p. 10.1117/12.765565.

[23] F. H. Imai, Technical Report: Multi-Spectral Image Acquisition and Spectral Reconstruction using a Trichromatic Digital Camera System Associated with Absorption Filters. Rochester: Munsell Color Science Laboratory, Rochester Institute of Technology, 1998.

[24] R. S. Berns, L. A. Taplin, M. Nezamabadi, and Y. Zhao, Technical Report: Modifications of a Sinarback 54 Digital Camera for Spectral and High-Accuracy Colorimetric Imaging: Simulations and Experiments. Rochester: Munsell Color Science Laboratory, Rochester Institute of Technology, 2004.

[25] R. S. Berns, L. A. Taplin, M. Nezamabadi, and M. Mohammadi, "Spectral imaging using a commercial color-filter array digital camera," in 14th Triennial Meeting, The Hague, 2005, pp. 743–750.

[26] F. H. Imai and R. S. Berns, "U. S. Patent 7,554,586 System and method for scene image acquisition and spectral estimation using a wide-band multi-channel image capture," 7,554,586, 2009.

[27] R. S. Berns, Theory and Practice of Dual-RGB Imaging. Rochester: Studio for Scientific Imaging and Archiving of Cultural Heritage, Rochester Institute of Technology, 2016.

[28] R. S. Berns, Spectral and Color Characteristics of Broncolor Pulso F4 Strobe with UVE Protection Dome. Rochester: Studio for Scientific Imaging and Archiving of Cultural Heritage, Rochester Institute of Technology, 2014.

[29] D. R. Wyble, "Next generation camera calibration target for archiving," in Archiving Conference, Riga: Society for Imaging Science and Technology, 2017, pp. 127–132.

[30] M. D. Fairchild and G. M. Johnson, "METACOW: A public-domain, high-resolution, fully-digital, noise-free, metameric, extended-dynamic-range, spectral test target for imaging system analysis and simulation," in IS&T/SID 12th Color Imaging Conference, Scottsdale, 2004, pp. 239–245.

[31] G. Wyszecki and W. S. Stiles, Color Science, 2nd ed. New York: John Wiley & Sons, 1982.

[32] D. R. Wyble and R. S. Berns, "Quantifying spectral sensitivity mismatch using a metameric color rule," Journal of Imaging Science and Technology, vol. 050402, pp. 1–6, 2019.

[33] P. L. Vora and H. J. Trussell, "Measure of goodness of a set of color-scanning filters," Journal of the Optical Society of America A vol. 10, pp. 1499–1508, 1993.

Acknowledgment

This research was supported by the Richard S. Hunter Professorship in Color Science, Appearance, and Technology.

Author Biography

Dr. Roy S. Berns is the Richard S. Hunter Professor in Color Science, Appearance, and Technology within the Program of Color Science at Rochester Institute of Technology, USA where he developed both M.S. and Ph.D. degree programs in Color Science. He received B.S. and M.S. degrees in Textiles from the University of California at Davis and a Ph.D. degree in Chemistry from Rensselaer Polytechnic Institute (RPI). Berns has received scientific achievement awards from the Inter-Society Color Council, the Society of Imaging Science and Technology, the Colour Group of Great Britain, and the International Association of Colour. Berns' main research focus is using color and imaging sciences for the visual arts, particularly paintings, including: 3-D imaging and computer-graphics rendering; spectral-based imaging, archiving, and reproduction; pigment mapping; and digital reconstructions of faded and darkened artwork.